FINITE ELEMENT MODELLING OF THE SELF-PIERCE RIVETING PROCESS

Dan Birsan[1]

[1] *"Dunarea de Jos" University of Galati, dbirsan@ugal.ro.*

Abstract: *The self-pierce riveting (SPR) process has gained prominence as a versatile joining technique in industries ranging from automotive to aerospace and beyond. Its unique ability to join dissimilar materials and its suitability for lightweight structures have made it a valuable alternative to traditional welding methods. In this context, finite element modeling (FEM) has emerged as a valuable tool for gaining insights into the complex phenomena occurring during SPR. This abstract provides an overview of the application of FEM in modeling the self-pierce riveting process. Key aspects covered include: geometry and meshing, material behavior, contact and friction, thermal effects, validation and optimization. Finite element modeling of the self-pierce riveting process offers a powerful means of gaining insights into the intricacies of this joining technique. It aids in the design, analysis, and optimization of SPR applications across a wide range of industries, contributing to the advancement of lightweight and durable structures.*

Keywords: *riveting, finite element, stress, strain*

1. Introduction

This work developed a finite element model containing two 7075-T6 aluminum plates welded by the self-pierce riveting process, the simulation results include temperature, strain, and stress distributions.

Aluminum alloy 7075-T6 is a high-strength aluminum alloy known for its excellent mechanical properties and is commonly used in various industries and applications, including: aerospace, defense, automotive, etc. Self-pierce riveting is a solid-state joining process that allows two or more sheets to be joined in an overlapping configuration.

Ren and co. Ref. [1] studied the effect of rivet arrangement on the strengths of lap joints and lap joint design methods. They proposed the concept of line load density to solve the problem that a varying rivet spacing and rivet edge distance will change the width of the sheet and thus the maximum load capacity, which is used as an index to study the effect of rivet spacing and rivet edge distance on the lap strength.

Jinrui and co. Ref. [2] presented the effect of edge riveting on the failure mechanism and mechanical properties of self-piercing riveted aluminum joints. They conducted an analysis of the influence of rivet placement on the structural strength, energy absorption capacity, and immediate stiffness of self-piercing riveted connections, employing the edge riveting technique.

Bradáč and co. Ref. [3] presented the evaluation of riveting force influence on the quality of riveted joint of aluminum alloy EN AW – 6016. The work consisted to evaluate the effect of the riveting force on the final quality of the riveted joint in the case of aluminum alloy.

2. Finite-element modeling

The numerical model developed provides a means to perform a comprehensive examination of the phenomena that occur during joint formation and the interactions that take place at the interface between the rivet surface and the plate. Following finite element analysis, the resulting findings must be aligned with experimental data for validation. In addition, validation can be achieved by comparing the results of the finite element analysis with those documented in the literature.

For the numerical analysis of the self-pierce riveting process (SPR), Simufact Forming software (Simufact Engineering GmbH, Hamburg, Germany) was used. This involved a coupled thermo-mechanical analysis to determine the temperature distribution, material deformations and stress patterns throughout the joining process.

Table 1: *Chemical composition of AA7075-T6*

Al	Mg	Si	Fe	Cu	Cr	Zn	Ti	Mn
87.1	2.1	max	max	1.2	0.18	5.1	max	max
91.4	2.4	0.4	0.5	2.0	0.28	6.1	0.2	0.3

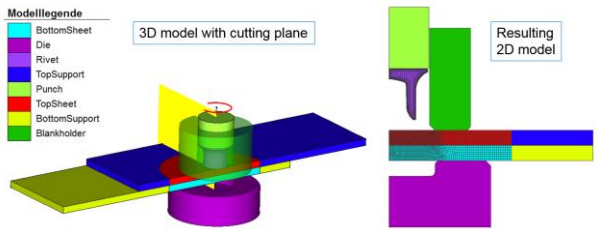

Figure 1: *Finite-element model*

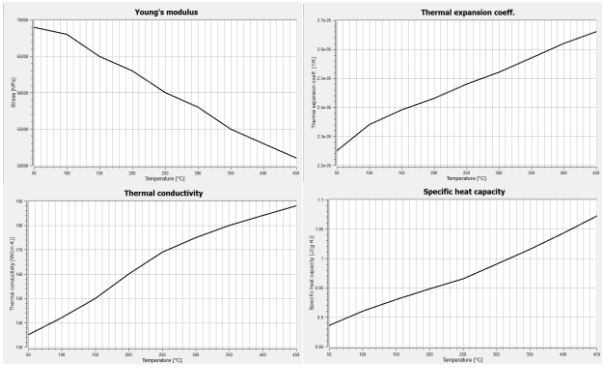

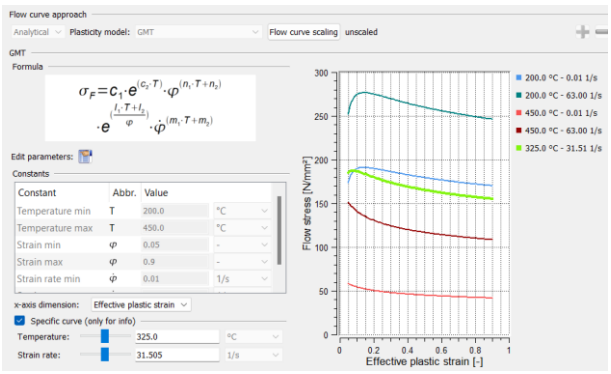

Figure 2: *AA 7075-T6 thermal and mechanical properties*

Boundary conditions were implemented to account for the impact of external factors on the model, thus preventing potential unrealistic demands that could occur in the regions of interest. The joining process required a press, which was defined as hydraulic press and a constant speed of 20.0 mm/s was specified.

In order to be able to control the friction pattern and the setting of the parameters in the joining process, the manual mode was selected. The combined friction model was used specifying a Coulomb friction coefficient of 0.1 and a plastic shear stress friction coefficient of 0.2.

The die set contains a spring-controlled blank holder that has been engaged with the punch to a stiffness of 400 N/mm. To model this behavior, a die spring has been added to the object box.

In the initial position of the empty support, the spring is released. The direction and value of the displacement that had to be taken into account in relation to the punch were selected. This means that as soon as it hits the sheet, the void support moves in the +z direction. The offset describes the distance between the initial position of the blank support and its final allowable position, both relative to the punch. An initial distance of 10 mm had to be left as offset between the bottom edge of the punch and the bottom edge of the blank.

The initial force has been set to 2.5 kN.

3. Results and Discussions

3.1. Equivalent stresses and plastic strain

The effective stresses that appear during the joining process are directly proportional to the

degree of deformation of the parts and inversely proportional to the temperature reached in them. In Figs. 3 and 4 show the equivalent stress during the joining process in two moments of time, at the end of the forming process and the second at the end of the release tool.

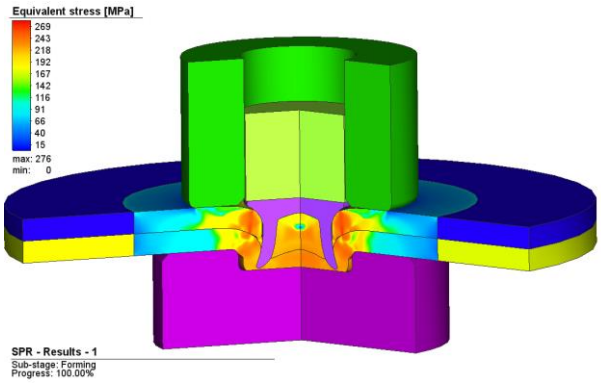

Figure 3: *Equivalent stress at the end of the forming process*

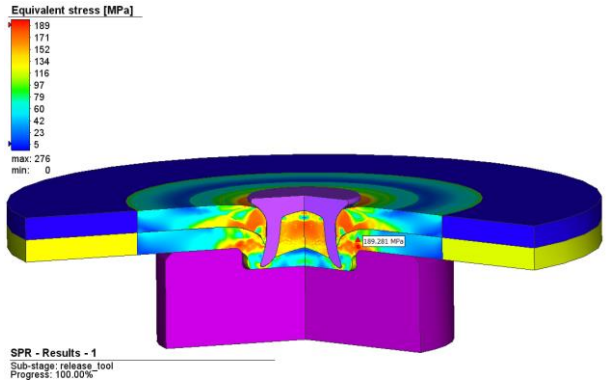

Figure 4: *Equivalent stress at the end of the release tool*

The effective stress of a welded joint depends on its temperature. It can be seen that the maximum stress occurs in the most deformed area, the maximum reaching 276 N/mm^2. The maximum residual stress in the sheets is 189 N/mm^2 and can be seen in Fig. 4.

Figures 5 and 6 show the plastic deformation of the riveted joint at two points in time, during and at the end of the forming process and the second at the end of the release tool.

The historical graph of the plastic deformation of the upper and lower sheets as well as the maximum values obtained can be seen in Fig. 7.

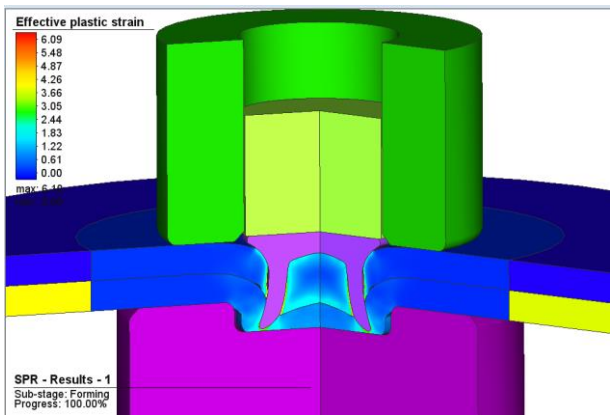

Figure 5: *Plastic strain at the end of the forming process*

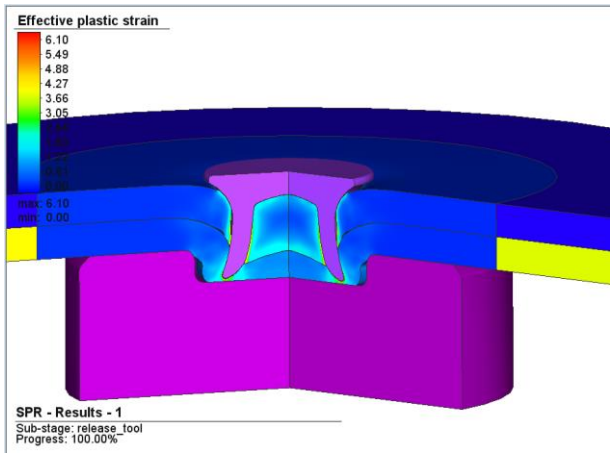

Figure 6: *Residual plastic strain at the end of the release tool*

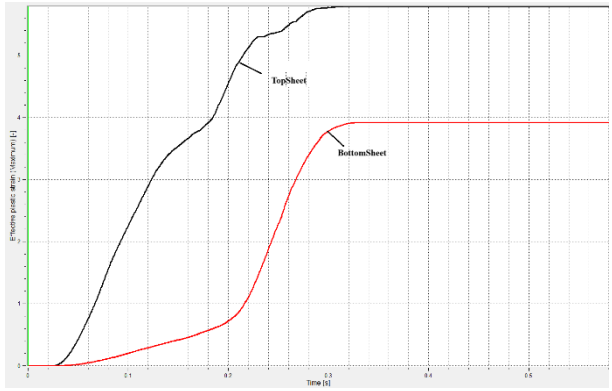

Figure 7: *Plastic strain history plot of the top and bottom sheets*

In Fig. 8 the evolution of the reaction force in the z-direction for die and punch throughout the riveting period can be seen. The maximum reaction force was 26.3 kN in punch and 31.7 kN in die.

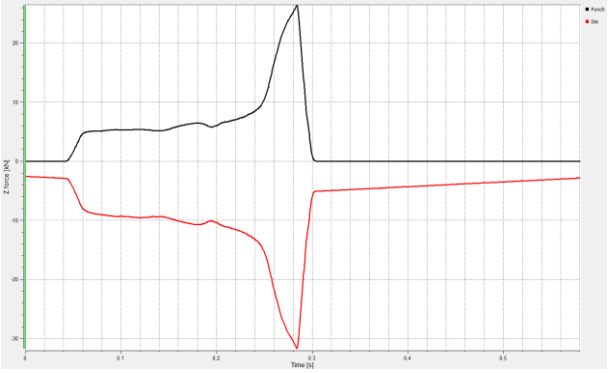

Figure 8: *Reaction force in z direction*

Fig. 9 shows the results of the automated measurements. The upper section gives information about the components, sheet thickness and material used. Various useful measurement values are shown below the measurements. The bottom minimum thickness value was used for the riveting completion criterion. As this value is 0.106 mm and therefore higher than the defined value of 0.1 mm, it did not cause the simulation to terminate.

Top sheet:	1.5 mm	DB.AlZnMgCu1.5_h2
Bottom sheet:	1.5 mm	DB.AlZnMgCu1.5_h2
	Name	**Geometry**
Rivet:	Rivet	Rivet
Blank holder:	Blankholder	Blankholder
Die:	Die	Die

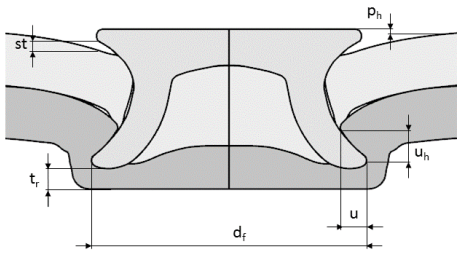

Measuring		
Name	**Variable**	**Value**
Interlock	u	0.341 mm
Vertical interlock	u_h	1.31 mm
Minimum bottom thickness	t_r	0.106 mm
Final rivet head position	p_h	0.293 mm
Gap distance	st	0.188 mm
Foot diameter	d_f	6.352 mm
Maximum punch force	Fs	29.0748 kN

Figure 9: *Measuring results*

4. Conclusions

The simulation of the rivet joining takes into account the changes in thermo-physical and mechanical properties of the 7075-T6 aluminum alloy as a function of temperature, leading to a very accurate solution in terms of the distribution and value of the thermal field, residual stress and plastic deformation. Three-dimensional analysis provides important data on the areas affected by the deformation process and the distribution of plastic deformations. The maximum value of the equivalent stress corresponds to the area affected by deformation. The simulation results were compared with data available in the literature and validated.

References

1. [Ren, 2023] Ren K., Han H., Xu W., Qing H., *The Effect of Rivet Arrangement on the Strengths of Lap Joints and Lap Joint Design Methods*, Journal of Applied Sciences, EISSN 2076-3417, 2023.
2. [Jinrui, 2023] Jinrui D., Chao C., *Effect of edge riveting on the failure mechanism and mechanical properties of self-piercing riveted* aluminium joints, Engineering Failure Analysis, Vol. 150, ISSN 1350-6307, 2023.
3. [Bradač, 2023] Bradač J., Sobotka J., *Evaluation of Riveting Force Influence on the Quality of Riveted Joint of Aluminium Alloy EN AW - 6016*, Manufacturing Technology, ISSN 1213-2489, 2023.
4. [Bîrsan, 2023] Bîrsan D. C., Paunoiu V., Teodor V., *Neural networks applied for predictive parameters analysis of the refill friction stir spot welding process of 6061-T6 aluminum alloy plates*, Journal of Materials, Vol. 16, Issue 13, 2023.
5. [Bîrsan, 2023] Bîrsan D. C., Gurău C., Marin F. B., Stefănescu C., Gurău G., Modeling of severe plastic deformation by HSHPT of as cast Ti-Nb-Zr-Ta-Fe-O Gum alloy for orthopaedic implant, Journal of Materials, Vol. 16, Issue 8, 2023.
6. [Birsan, 2022] Birsan D. C., Simion G., *Numerical modelling of thermo-mechanical effects developed in resistance spot welding of E304 steel with copper interlayer*, Annals of "Dunarea de Jos" University, Fascicle XII, Welding Equipment and Technology, 2022, Vol. 33, pp. 89-94.
7. [Birsan, 2022] Birsan D., *Simulation of a refill friction stir spot welding process*, New Technologies and Products in Machine Manufacturing Technologies Journal, P - ISSN-1224-029X, E - ISSN-2247-6016.
8. [Birsan, 2021] Birsan D., *Thermal field and residual stresses during the resistance spot welding process*, New Technologies and Products in Machine Manufacturing Technologies Journal, P - ISSN-1224-029X, E - ISSN2247-6016.

9. [Birsan, 2021] Birsan D. C., Simion G., Voiculescu I., Scutelnicu E., *Numerical Model Developed for Thermo-Mecahnical Analysis in AlCrFeMnNiHf0.05–Armox 500 Steel Welded Joint*, Annals of "Dunarea de Jos" University, Fascicle XII, Welding Equipment and Technology, 2021, Vol. 32, pp. 37-46.
10. [Florescu, 2018] Florescu S.N, Mihăilescu D., Birsan D.C., Mocanu C.I., *Researches on the thermal fields analysis at MAG-M mechanized butt welding with solid wire*, The Annals of Dunarea de Jos University of Galati, Fascicle XI, Shipbuilding, Year XXXIV, 2018, ISSN 1221-4620, Galati University Press.
11. [Birsan, 2017] Birsan D., *Finite element analysis of residual stresses in naval structures due to multiarc welding process*, New Technologies and Products in Machine Manufacturing Technologies Journal, ISSN-2247-6016, pag. 234-242
12. [***, 2019] ***, *Simufact Forming Theory manual*. Champaign. Computational Applications and System Integration Inc., 2019.